

Templating the near-surface liquid electrolyte: *In situ* surface x-ray diffraction study on anion/cation interactions at electrified interfaces

Hubert Keller,^{1,*} Martino Saracino,^{2,3} Hai M. T. Nguyen,² and Peter Broekmann²

¹*Institut für Theoretische und Angewandte Physik, Universität Stuttgart, Pfaffenwaldring 57, 70569 Stuttgart, Germany*

²*Department of Chemistry and Biochemistry, University of Berne, Freiestrasse 3, 3012 Berne, Switzerland*

³*Institut für Physikalische and Theoretische Chemie, Universität Bonn, Wegelerstr. 12, 53115 Bonn, Germany*

(Received 21 September 2010; published 17 December 2010)

We present an *in situ* surface x-ray diffraction study on the structuring impact of an anion-modified electrode surface on the near-surface liquid electrolyte. This templating effect of the so-called inner Helmholtz layer of specifically adsorbed anions affects not only the interfacial structure parallel to the surface normal by layering the liquid in the near-surface regime but induces moreover a lateral ordering of water dipoles and solvated counter ions in the so-called outer Helmholtz layer. In this respect, we observe a symmetry transfer from the inner Helmholtz layer into the liquid electrolyte next to the electrode surface. Our prototypical model system is a Cu(100) surface on which chloride adsorbs under the formation of a simple $p(1 \times 1)$ adlayer phase (this notation refers to the fcc unit cell of Cu) that serves as structural template for the coadsorption of monovalent potassium and hydronium cations from the acidified supporting electrolyte. A layer of interfacial water is interpreted as a part of the remaining solvation shell of potassium cations in the outer Helmholtz layer.

DOI: 10.1103/PhysRevB.82.245425

PACS number(s): 68.08.-p, 61.05.cf, 68.37.Ef, 82.45.Mp

I. INTRODUCTION

The atomic-scale characterization of electrified solid/liquid model interfaces has been a key topic in the field of surface electrochemistry for almost three decades.¹ One of the most fundamental scientific challenges in this context was and still is the ultimate correlation between the full three-dimensional (3D) structure of the interface and its reactivity. Solving this problem is vital for various branches of applied and fundamental electrochemistry such as electrocatalysis,^{2,3} corrosion, corrosion protection, and electroplating.⁴

Most of the previous experimental work based on structure-sensitive methods such as *in situ* scanning probe microscopy and surface x-ray diffraction (SXRD) was, however, restricted to the solid electrode (=metal surface including the inner Helmholtz layer of chemisorbed ions as the outermost part of the solid next to the liquid electrolyte) thereby neglecting the electrolyte side of the electric double layer (=outer and diffuse Helmholtz layer as the outermost part of the liquid electrolyte next to the solid electrode).¹ Solvated counter ions accumulate here and counterbalance charges of opposite sign either at the bare metal electrode surface or if present at the layer of specifically adsorbed ions (inner Helmholtz layer).⁵ In particular, halide anions (Cl^- , Br^- , I^-) typically show a strong tendency toward chemisorption on metallic electrode surfaces leading to condensed and laterally well-ordered monolayer phases.¹ These are known to affect both the rate and the mechanism of electron^{6,7} and ion transfer reactions⁸ taking place at the interface.

While the lateral structure of these two-dimensional (2D) halide phases at the solid/liquid interfaces were found to be identical to the respective solid/vacuum interface notable differences in the structure perpendicular to the surface normal were reported for both experimental environments.⁹⁻¹² Not only the spacing between the topmost anion/metal layers are

affected by the presence of the outer Helmholtz layer of solvated cations and water dipoles but more remarkably even the metal/metal layer separations inside the electrode.⁹⁻¹¹ All these structural differences originate from the fact that the specifically adsorbed anions find their binding partners not solely in the atoms of the underlying metal substrate surface but coordinate in addition to water dipoles and solvated cations residing in the outer Helmholtz layer thereby sandwiching the specifically adsorbed anions in the inner Helmholtz layer.

Prototypical model systems to study these structural phenomena in both experimental environments are fcc(100) surfaces of Cu on which most halides adsorb under the formation of simple low-order commensurate $p(1 \times 1)$ adlayers^{9,13-18} whose $p4mm$ symmetry is not restricted to the adlayer itself but extends into the first few substrate layers here introducing a slight subsurface buckling.^{10,11,19}

For Cu(100) in 10 mM HCl electrolyte solution previous studies by Huemann *et al.*⁹ and Gründer *et al.*¹¹ consistently report a metal/chloride interlayer separation of $d_{\text{Cu-Cl}} = 1.880 \text{ \AA}$ ⁹ and $d_{\text{Cu-Cl}} = 1.856 \text{ \AA}$ ¹¹ that is expanded by about 17% with respect to the halide-copper spacing of the corresponding $p(1 \times 1)$ chlorine adsorption layer under UHV conditions.¹² This observation clearly proves the specific impact of the outer Helmholtz layer on the entire out-of-plane structure of the interface.

Please note that in the literature the $p(1 \times 1)$ -Cl adlayer is often referred to as $c(2 \times 2)$ phase. However, this notation involves an inappropriate lowering of the substrate symmetry by choosing a body-centered tetragonal cell for Cu that leads consequently to a larger adlayer cell with $a_{c(2 \times 2)} = 5.12 \text{ \AA}$. The $p(1 \times 1)$ adlayer notation is based on a conventional face-centered-cubic unit cell of the Cu substrate with $a_{p(1 \times 1)} = 3.61 \text{ \AA}$ and describes also the smallest possible unit cell of the adlayer.

Compared to the level of knowledge we have from the structural properties of the inner Helmholtz layer far less is

known about the ordering and spatial distribution of ions and water dipoles in the outer Helmholtz layer on the electrolyte side. Most of the experimental^{20–22} and theoretical work^{23,24} in this field considers the layering of water perpendicular to the charged metal/liquid interface. For a Ag(111)/electrolyte interface in 0.1 M NaF solution Toney *et al.* report interfacial water layers that reveal a potential-dependent ordering that extends three molecular dimensions into the liquid electrolyte phase.^{20–22} These interfacial water layers were found to be significantly denser than the corresponding bulk electrolyte phase reaching a compression factor of up to 2.^{20–22} Lateral order within these inner water layers, however, has been considered as negligible.^{20–22} A structuring effect originating from the fluoride anions or the sodium cations has also not been taken into account in this study. Their presence in the outer and diffuse Helmholtz layer, however, might disturb the spatial distribution of water next to the electrode surface due to local solvation effects thereby disrupting the common H-bonded network of interfacial water.^{25–27}

Out-of-plane ordering phenomena of interfacial water are well documented not only for metal/electrolyte but also mineral/water interfaces.²⁸ Crucial for the ordering of the interfacial water is the particular surface structure and composition of the mineral that determines the density profile of water perpendicular to the surface.

In this contribution we will demonstrate by means of *in situ* SXR D measurements, however, that water molecules and solvated ions in the outer Helmholtz layer do not solely show an order perpendicular to the interface but reveal in addition a certain positional and lateral order parallel to the surface. In our model system, the ordering process is driven by a *templating effect* of the chemisorbing anions in the inner Helmholtz layer on those water dipoles and ionic species in the outer Helmholtz layer. The adlayer symmetry is here transferred not only into the underlying solid metal substrate as previously reported by Saracino *et al.*¹⁰ and Gr nder *et al.*¹¹ but is transferred moreover into the near-surface regime of the liquid electrolyte.

While previous *in situ* SXR D studies on the interfacial water layers next to an anion-free Ag(111) electrode were mainly focused to an analysis of the specular (00L) rod intensities,^{20–22} we further include the (10L) and (12L) adlayer rods (ADRs) and the (20L) crystal truncation rod (CTR)²⁹ into our full 3D structure analysis. X-ray intensities along the (10L) and (12L) rods originate only from diffraction from the entire interfacial regime that is structurally affected by the inner Helmholtz layer of chemisorbed anions. Due to the common fcc reflection conditions there are no intrinsic diffraction intensities from the Cu bulk material at these positions in reciprocal space. Important to state is that both ADRs and CTRs are sensitive not only to relaxation and reconstruction phenomena in the solid electrode surface^{12–14} but contain additional information on the lateral ordering of the solvated ions in the outer Helmholtz layer on electrolyte side as direct consequence of the symmetry transfer from the anion layer into the near-surface liquid phase.

II. EXPERIMENT

The x-ray scattering experiment reported here has been performed in an electrochemical cell utilizing a hanging

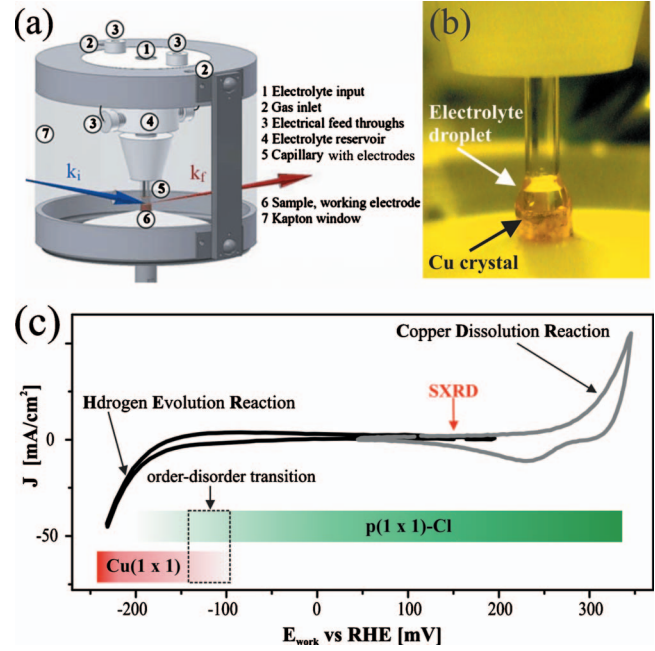


FIG. 1. (Color) (a) Schematic drawing of the electrochemical SXR D cell. k_i and k_f are the wave vectors of the incoming and diffracted x-rays, respectively; (b) picture of the copper sample in the hanging droplet configuration; (c) cyclic voltammogram (CV) of Cu(100) in the 5 mM H_2SO_4 /10 mM KCl electrolyte indicating the stability range of the $p(1 \times 1)$ -Cl chemisorption layer (inner Helmholtz layer); CV obtained in the *in situ* SXR D cell.

droplet configuration^{10,30–32} that allows a stable potential control during the SXR D experiment (Fig. 1). The stability range of the $p(1 \times 1)$ -Cl adlayer phase on Cu(100)^{1,11,15–17} within the potential window of copper in 5 mM H_2SO_4 /10 mM KCl solution is shown in Fig. 1(c). In the present paper we focus our 3D structure analysis on the interface at a potential of $E_{\text{work}} = +150$ mV (Fig. 2). Under these conditions the ordering in the outer Helmholtz layer is developed most since the $p(1 \times 1)$ -Cl reveals a chloride surface coverage close to saturation limit of $\Theta = 0.5$ ML (ML = monolayer, 1 ML = 1 atom per Cu atom of the surface layer)^{1,11} so that there is no disturbance in the ordering of cations by vacancies as structural defects within the anionic inner Helmholtz layer (Fig. 2). These point defects appear in the chloride layer at more negative potentials close to the

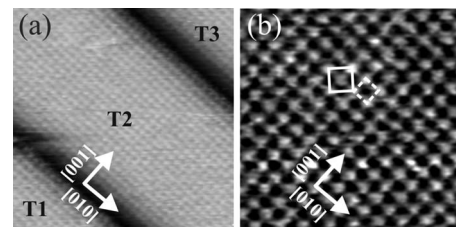


FIG. 2. (a) Scanning tunneling microscope image of the Cu(100) surface morphology in the presence of the $p(1 \times 1)$ -Cl adlayer (inner Helmholtz layer), T1–T3 indicate different terraces separated by monatomically high substrate steps, $13 \text{ nm} \times 13 \text{ nm}$, $I_t = 5 \text{ nA}$, $U_{\text{bias}} = -312 \text{ mV}$; (b) atomic structure of the $p(1 \times 1)$ -Cl adlayer on Cu(100), $4.2 \text{ nm} \times 4.2 \text{ nm}$, $I_t = 0.67 \text{ nA}$, $U_{\text{bias}} = 81 \text{ mV}$.

potential-induced order-disorder transition within the $p(1 \times 1)$ -Cl phase.^{11,16,17}

The synchrotron beam of 20 keV was provided by beam-line X04SA at the Swiss Light Source (SLS). As sample we used a Cu crystal that was 5 mm in diameter and polished to within 0.2° of the crystallographic (100) plane. The bulk mosaic was 0.07° at the (202) reflection. For $E_{\text{work}} = +150$ mV we measured the specular (00L) rod, the (20L) CTR and the (10L), the (12L) ADRs up to a maximum normal momentum transfer of $q_z = 7.48 \text{ \AA}^{-1}$, which is equivalent to 4.3 reciprocal lattice units. The results are presented with reference to the crystallographic bulk notation of copper with a cubic face-centered unit cell and a lattice constant of $a_{\text{Cu}} = 3.61 \text{ \AA}$ at room temperature.

III. RESULTS AND DISCUSSION

Our x-ray diffraction analysis is based on the measurement of 260 symmetrically independent CTR and ADR reflections [see Figs. 3(a) and 3(b)] at room temperature in z -axis geometry.³³ The data set was collected using a PILATUS II pixel detector³⁴ with a dynamic range of 10^6 for each of its 487×195 pixels. The 2D PILATUS detector technology appears advantageous, in particular, in the combination with an electrochemical setup since we expect significantly lower signal to noise ratios compared to respective solid/vacuum interfaces.^{35,36} A careful background correction and a fast data collection appear therefore essential for the success of the experiment. The data was collected by rotating the sample around its surface normal hereby measuring a series of 2D areas of diffracted intensity around the region of a surface rod. This series was then integrated along the scan direction of the rotation and represents a volume of reciprocal space that contains typically about a quarter of a surface rod ($\Delta q_z = 0.75$) with its background. Slices of that volume are then used to retrieve the intensity and background for a certain q_z value along a rod of scattering. In contrast to the data collection with 2D detectors, data collection with conventional point detectors produce only integrated intensities for one specific q_z value per scan.

We corrected integrated intensities for background scattering, polarization, and Lorentz factor. Background was mainly caused by the electrolyte droplet and by the Kapton foil that was used to seal the electrochemical cell from air electrolyte [Fig. 1(a)].

The experimental error of the diffraction intensities includes the error of the background correction, their standard deviation, and the error resulting from the reproducibility of symmetry equivalent reflections that produced an internal R value of 18% based on $|F|^2$ (F =scattering amplitude) for all reflections.

Figures 3(a) and 3(b) show the complete set of data points represented by symbols with error bars. Our best fit to the measured structure factors is given by the solid lines. The dashed line in Fig. 3(b) illustrates the model of a recent analysis of Cl on Cu(100) by Gründer *et al.*¹¹ The 2D surface diffraction pattern observed in the present study is depicted in the inset of Fig. 3(b). Each symbol indicates a rod parallel to the surface normal direction along which the scattered

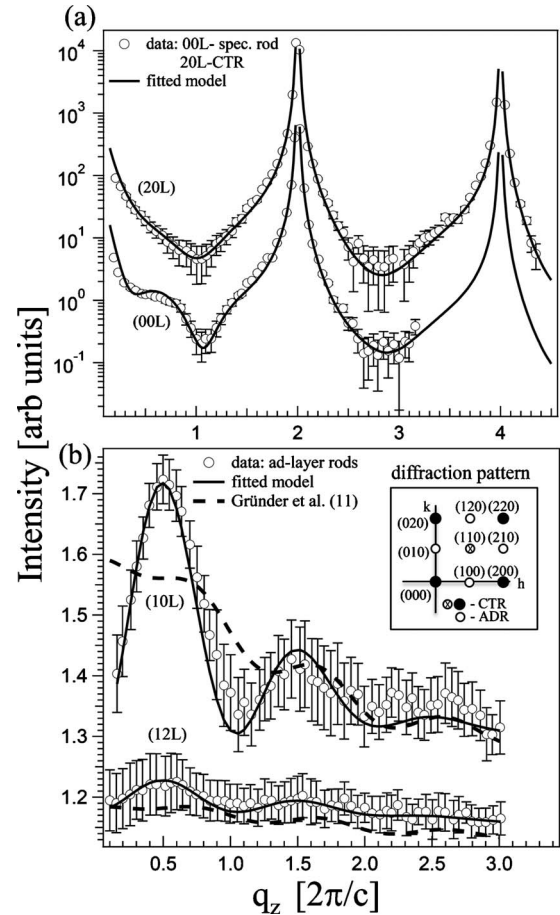


FIG. 3. (a) Experimental data and best fit of the (00L) specular rod and the (20L) crystal truncation rod, $E_{\text{sample}} = +150$ mV (CTR: crystal truncation rod; ADR: adlayer rod); (b) experimental data and best fit of the (10L) and (12L) adlayer rods in comparison with model (dashed line) proposed by Gründer *et al.*,¹¹ $E_{\text{sample}} = +150$ mV. The unit $2\pi/c$ is the length of the momentum transfer vector perpendicular to the surface, q_z , with $c = a_{\text{Cu}} = 3.61 \text{ \AA}$ as the lattice constant of Cu. The inset indexes the reciprocal lattice points in the $(HK0)$ plane with reference to the conventional fcc unit cell of copper.

x-ray intensity is distributed. The full circles and those with a cross represent CTRs, the open circles indicate ADRs that are solely related to scattering from the interfacial regime, which is directly affected by the chloride adlayer without any contributions of the copper bulk material.

Our structure model leads to a significantly improved geometric description of electrified solid/liquid interfaces in general that extends existing models by far⁹⁻¹¹ by considering the lateral and positional ordering within the entire electric double layer.

Our model requires only six structural parameters that include the topmost Cu layer spacing $d_{\text{Cu2-Cu1}}$, the separation of the chloride chemisorption layer (inner Helmholtz layer) from the Cu(100) substrate $d_{\text{Cu1-Cl}}$, the separation between the interfacial water layer SL and the inner Helmholtz layer $d_{\text{Cl-SL}}$ and finally the spacing between the cation layer and the interfacial water layer $d_{\text{SL-CaL}}$. The cation layer consists of positively charged potassium and hydronium [Figs. 4(a)

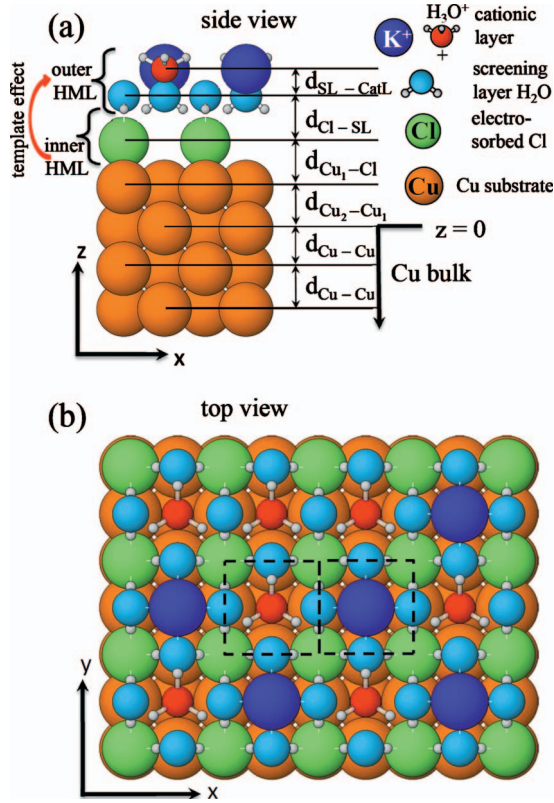


FIG. 4. (Color) Full 3D structure model of the metal/electrolyte interface of Cu(100) in; (a) out-of plane structure (side view); (b) in-plane structure (top view). The dashed lines indicate the size and position of the Cu bulk unit cell. HML: Helmholtz layer.

and 4(b)]. Further parameters are the occupancies of the anionic chloride layer Θ_{Cl} and that of K^+ in the cation layer Θ_{K^+} . The occupancy of the water layer is twice that of Cl and that of the cation layer is normalized to Θ_{Cl} . From this follows: $\Theta_{\text{H}_3\text{O}^+} = \Theta_{\text{Cl}} - \Theta_{\text{K}^+}$.

Cationic K^+ and H_3O^+ species are both present in the electrolyte and compete therefore for the same fourfold hollows as their preferred adsorption sites on the anionic inner Helmholtz layer [Fig. 4(b)]. A clear preference of these cations for those hollow sites can directly be deduced from the intensity distribution in both ADRs at low- q_z values [Fig. 3(b)]. It is the presence of these cationic species in the fourfold hollows sites of the inner Helmholtz layer that introduces an additional annihilation condition into the scattering experiment thus explaining the particularly low intensity at low- q_z values and it explains moreover also the overall oscillation in the ADRs along q_z . It is this unique feature of the electrochemical environment that explains the pronounced differences to the intensity distribution of the ADRs reported by Tolentino *et al.* for the respective Cu(100)/Cl/vacuum interface.¹²

For a given electrode potential and $\text{K}^+/\text{H}_3\text{O}^+$ concentration in the bulk electrolyte a defined ratio of $\text{K}^+/\text{H}_3\text{O}^+$ occupancies is established onto of the chloride $p(1 \times 1)$ lattice with Θ_{K^+} and $\Theta_{\text{H}_3\text{O}^+}$ as partial cation occupancies. Both sum up to Θ_{Cl} as the total cation occupancy thus guaranteeing charge neutrality within the electric double layer. Note, however, that the XRD experiment can in fact not discriminate

TABLE I. Structural parameters of the Cu(100)/electrolyte interface according to the best fit of our x-ray data. The number in brackets indicates the error to the value next to it with reference to its last digit.

Layer spacing, d_{x-y}	In units of $(a/2)$, In (\AA)
$d_{\text{SL-CatL}}$	0.72 (4), 1.30(7)
$d_{\text{Cl-SL}}$	1.18 (6), 2.13(11)
$d_{\text{Cu1-Cl}}$	1.10 (3), 1.99(5)
$d_{\text{Cu2-Cu1}}$	1.008 (4), 1.820(7)
$d_{\text{Cu-Cu}}$	1.000, 1.805
$d_{\text{Cu-Cu}}$	1.000, 1.805
Layer occupancy, θ	In ML
$\Theta_{\text{Cl}} = \frac{1}{2}\Theta_{\text{SL}}$	0.45 (5)
$\Theta_{\text{K}^+} = \theta_{\text{K}^+} \cdot \Theta_{\text{Cl}}$	0.15 (7)
$\Theta_{\text{H}_3\text{O}^+} = \Theta_{\text{Cl}} - \Theta_{\text{K}^+}$	0.30 (7)
Debye-Waller factor, B	In \AA^2
$B(\text{K}^+, \text{H}_3\text{O}^+, \text{H}_2\text{O})$	8.4 (9)

between H_2O and H_3O^+ . Our fit procedure considers only the oxygen as scattering centers. Other scenarios are possible where H_2O is present within the cation layer instead of H_3O^+ . Under these conditions the overall charge neutrality is reached by assuming an excess of H_3O^+ species within the diffuse part of the double layer.

Our (simplified) model assumes that both cations are statistically distributed on the fourfold hollow sites of the chloride lattice in order to preserve the $p4mm$ symmetry on average. It is the conservation of this symmetry [Fig. 3(b)] that excludes long range ordering of either K^+ or H_3O^+ species within the cation layer, which, in turn, would result into an additional superstructure beyond the observed $p4mm$ symmetry of the $p(1 \times 1)$ structure.

The particular structure of the cation layer as presented in Fig. 4 should not be regarded as a static one with potassium and hydronium species fixed on distinct adsorption sites but as highly dynamic one. The diffraction experiment averages statistically over a huge number of similar structural realizations of the cation layer. Potassium and hydronium cations undergo pronounced exchange processes with the bulk electrolyte as prerequisite for positional changes through the electrolyte phase. As a physically meaningful parameter we therefore introduced a pseudo-Debye-Waller factor B (Table I) into our structure model as a generic term that comprises not only the thermal motion of the adsorbed species in the outer Helmholtz layer perpendicular to the interface but comprises in addition the huge exchange dynamics of nonchemisorbed particles in the outer Helmholtz layer with the liquid electrolyte phase. Similar to the thermal motion these reversible adsorption/desorption processes represent also distinct displacements of scattering centers (oxygen or potassium in this case) as a function of time thus leading to an attenuation of the scattered x-rays and by this to an in-

crease in the diffuse background intensity. It was sufficient to fit only one isotropic pseudo Debye-Waller factor for potassium, for the oxygen of the hydronium and for the oxygen of the interfacial water layer together in order to achieve a good agreement between experimental data and fit. The choice of an isotropic Debye-Waller factor is justified by the fact that a lateral as well as vertical exchange of cations and water molecules should be allowed on the liquid side of an interface. This Debye-Waller factor reveals a value of $8.4(9) \text{ \AA}^2$ (Table I) which is reasonably high for particles that experience a dynamic exchange at the solid/liquid interface. The value of $8.4(9) \text{ \AA}^2$ is three times larger than those found by Gr nder *et al.*¹¹ for various different atoms of in their inner Helmholtz layer. The structure of the outer Helmholtz layer was not included in their model.

Since the interlayer separation between cation and the interfacial water layer [$d_{\text{CL-CatL}}=1.30(7) \text{ \AA}$] is significantly smaller than the one between the chloride and the water with $d_{\text{CL-SL}}=2.13(11) \text{ \AA}$ we interpret this interfacial water layer as an essential part of the remaining potassium solvation shell at the interface with oxygen of water dipoles oriented toward the cations while hydrogen points toward the inner Helmholtz layer thus allowing H bonding to the chloride. Note that it is not possible to derive the absolute orientation and tilt of the water species from our x-ray scattering experiments as shown schematically in Fig. 3(a) due to the weak scattering power of hydrogen.

The small interlayer spacing of $d_{\text{SL-CatL}}=1.30(7) \text{ \AA}$ suggests that the potassium cations have to be considered to be more embedded into an interfacial water matrix than really being separated from the chloride layer by an extra water layer. O coordination to the metal cations, H bonding to the chloride, and the interaction of water dipoles with the E field originating from the anion-cation-layer separation might disturb cooperatively the H-bonded water network at the interface so that the resulting water structure significantly differs from the bilayer structure motif known from water adsorption on pure metal surfaces²⁵⁻²⁷ or from high-pressure icelike phase at the interface as reported for the dense interfacial water layers next to a Ag(111) electrode.²⁰⁻²² While for the Ag(111) electrode Toney *et al.*^{21,22} report an areal density of interfacial water with $\Gamma=1.55 \times 10^{15} \text{ cm}^{-2}$ for a negative ($E_{\text{work}}=-230 \text{ mV}$) and $2.6 \times 10^{15} \text{ cm}^{-2}$ for a positive electrode polarization ($E_{\text{work}}=+520 \text{ mV}$), respectively, we find an areal density of water within the electric double layer of $\Gamma=1.14 \times 10^{15} \text{ cm}^{-2}$ that matches well the one of bulk water with $\Gamma=1.15 \times 10^{15} \text{ cm}^{-2}$.^{21,22} Basis for this calculation is the combined surface coverage of water and hydronium cations from our structure model [Fig. 3(b)] that amounts to $\Theta_{\text{SL}}=0.45 \text{ ML}$ and $\Theta_{\text{H}_3\text{O}^+}=0.3 \text{ ML}$, respectively. Consequently, not the water density at the interface is impacted here by the presence of the solid electrode surface but only its spatial distribution due to an extension of the adlayer symmetry into the near surface electrolyte phase [Fig. 3(b)]. In the view of surface electrochemistry, we identify the interfacial water together with the cation layer as the outer Helmholtz layer⁵ in terms of an ordered liquid phase whose structure is governed by the templating inner Helmholtz layer next to it.

Our new model also confirms on a qualitative basis the previously reported trend toward huge metal/halide inter-

layer separations⁹⁻¹¹ as a characteristic of the electrochemical environment. The value of $d_{\text{Cu-Cl}}=1.99(5) \text{ \AA}$ (Table I) found in the present study is expanded by 20% with respect to the corresponding $p(1 \times 1)$ chlorine adsorption layer under UHV conditions.¹² This value is 3% higher than those reported in the previous studies.^{9-11,37} This deviation in the metal/halide interlayer separation could arise from differences in the electrolyte composition. While in the previous studies pure 10 mM HCl solutions were used as supporting electrolyte we introduced potassium chloride as anion and cation source besides the sulfuric acid. Note that the sulfate anions do not play any role for the specific anion adsorption process when halide anions are present. For the cation adsorption on top of the inner Helmholtz layer, however, we realized in the present study a competitive situation where both hydronium and potassium compete for the same adsorption sites while in the former studies only hydronium was present as cationic species in the outer Helmholtz layer. One might argue that the chemical composition in the outer Helmholtz layer has direct impact also on the metal/halide separation (chemistry dependence). Recent *in situ* SXDR measurements on the adsorption of divalent calcium cations onto the same $p(1 \times 1)$ -Cl lattice on Cu(100) seem to confirm this latter hypothesis.³⁸

Also confirmed by this present study is the surface relaxation of the topmost copper layers that is slightly expanded by $0.015(7) \text{ \AA}$ with reference to the bulk Cu spacing that is adopted by deeper Cu layers. The same trend was found in the SXRD study of Huemann *et al.*⁹ with an expansion of $0.040(7) \text{ \AA}$. The recent SXRD study by Gr nder *et al.*¹¹ proposes no relaxation of substrate layer separations within the error of that parameter that amounts to 0.025 \AA . Instead, they suggest a buckling of the second Cu layer with amplitude equal to the error of its average position.¹¹

No such buckling could be detected in our analysis since the involved displacements of Cu are too small to adjust or improve the fit of the model significantly. In particular, the ADR data are not reproduced up to a momentum transfer $q_z=1.5$ by the ‘‘buckling’’ model alone.¹¹ CTR data are mostly insensitive to this fine structural feature. The characteristic intensity distribution along the ADRs is typical for centered double adlayer systems where the position of the broad peaks determines their separation and distance from the relaxed Cu surface. Therefore, it is the introduction of an additional layer like the cation layer that reproduces the characteristic intensity distribution along the ADRs and the specular rod considerably better than all other proposed models in the literature, although our model is based on even fewer fitting parameters.

A satisfying agreement between the experimental data and the fit is achieved, in particular, at low- q_z values only by including the outer Helmholtz layer into the model. We cannot exclude a subsurface buckling in the present case but its amplitude would be too small in order to be a significant geometric feature of the model.

The uniqueness of our new model and statistical significance of the results are expressed by the goodness of fit (GoF)³⁹ that equals to 0.95. Values close to one imply that the extent of the match between observations and estimates is in accord with the error variance. Within the range of the

errors and for the given set of fit parameters there is then barely any more significant information contained in the data which would change the model significantly, for instance by introducing a subsurface buckling. The model was fitted to all data simultaneously by using the following kinematic approximation calculating its intensity contribution for all experimental (hkl) reflections,

$$I(\mathbf{q}) = S \cdot \left| \left(1 - e^{-2\pi i q_3 - \mu} \right)^{-1} \sum_m f_{\text{Cu}}(\mathbf{q}) e^{2\pi i \mathbf{q} \cdot \mathbf{r}_m^{\text{Cu, bulk}}} \right. \\ \left. + \sum_n f_{\text{Cu}}(\mathbf{q}) e^{2\pi i \mathbf{q} \cdot \mathbf{r}_n^{\text{Cu, surface}}} + 2\Theta_{\text{Cl}} f_{\text{Cl}}(\mathbf{q}) e^{2\pi i \mathbf{q} \cdot \mathbf{r}^{\text{Cl}}} \right. \\ \left. + e^{-Bq^2/(4\pi)^2} 2\Theta_{\text{Cl}} \left[\sum_p f_{\text{H}_2\text{O}}(\mathbf{q}) e^{2\pi i \mathbf{q} \cdot \mathbf{r}_p^{\text{H}_2\text{O}}} \right. \right. \\ \left. \left. + 2\Theta_{\text{K}^+} f_{\text{K}^+}(\mathbf{q}) e^{2\pi i \mathbf{q} \cdot \mathbf{r}^{\text{K}^+}} \right. \right. \\ \left. \left. + (1 - 2\Theta_{\text{K}^+}) f_{\text{H}_3\text{O}^+}(\mathbf{q}) \cdot e^{2\pi i \mathbf{q} \cdot \mathbf{r}^{\text{H}_3\text{O}^+}} \right] \right|^2$$

With $I(q)$: intensity, S : scaling factor, q : momentum transfer, q_3 : momentum transfer perpendicular to the sample surface, μ : penetration depth of x-rays in angstrom, $f_x(q)$: atomic form factor of atom x , r_x : vector in relative coordinates pointing from origin of unit cell to atom x , B : Debye-Waller factor in square angstrom, Θ_x : occupancy of atom x in ML.

The upper line in the equation calculates the bulk contribution of scattering for the CTR and specular data. The second line contains the scattering term for relaxed Cu surface

layers and the adsorbed Cl, both are solely surface scattering contributions. The same is true for the scattering of the water layer and the mixed cation layer whose occupancy is normalized to that of the underlying Cl layer. In addition, a Debye-Waller term is added to calculate the scattering for this part of the structure.

IV. CONCLUSIONS

This study provides an extension of existing models of the electric double layer by considering the lateral ordering of solvated cations and interfacial water within the so-called outer Helmholtz layer induced by the lattice of chemisorbed chloride anions in the inner Helmholtz layer. Periodic modulations in the electrostatic potential at the anion layer have been identified as driving force for the lateral ordering of solvated cations that favor fourfold hollows as adsorption sites in the anion layer. Prototypical model system to study ordering processes on electrolyte side next to a charged electrode surface is a $p(1 \times 1)$ chloride layer on Cu(100) whose $p4mm$ symmetry is transferred into the near-surface liquid electrolyte phase.

ACKNOWLEDGMENTS

The authors gratefully acknowledge the support of Steven Leake, Michael Lange, Dominik Meister, and of the beamline manager Philip Willmott at the beamline X04SA of the SLS. We also thank the BASF SE (Electronic Materials) for financial support.

*Corresponding author. FAX: ++49 711 685 55264; keller@itap.uni-stuttgart.de

¹O. M. Magnussen, *Chem. Rev.* **102**, 679 (2002).

²N. M. Marković and P. N. Ross, Jr., *Surf. Sci. Rep.* **45**, 117 (2002).

³D. S. Strmcnik, P. Rebec, M. Gaberscek, D. Tripkovic, V. Stamenkovic, C. Lucas, and N. M. Marcovic, *J. Phys. Chem. C* **111**, 18672 (2007).

⁴T. P. Moffat, D. Wheeler, M. Edelstein, and D. Josell, *IBM J. Res. Dev.* **49**, 19 (2005).

⁵Southampton Electrochemistry Group, *Instrumental Methods in Electrochemistry*, Ellis Horwood Series in Physical Chemistry (Ellis Horwood Ltd., 1990).

⁶C. Safarowsky, K. Wandelt, and P. Broekmann, *Langmuir* **20**, 8261 (2004).

⁷D. T. Pham, K. Gentz, C. Zörlein, N. T. M. Hai, S.-L. Tsay, B. Kirchner, S. Kossmann, K. Wandelt, and P. Broekmann, *New J. Chem.* **30**, 1439 (2006).

⁸W. Polewska, R. J. Behm, and O. M. Magnussen, *Electrochim. Acta* **48**, 2915 (2003).

⁹S. Huemann, N. T. M. Hai, P. Broekmann, K. Wandelt, H. Zajonz, and H. Dosch, *J. Phys. Chem. B* **110**, 24955 (2006).

¹⁰M. Saracino, P. Broekmann, K. Gentz, M. Becker, H. Keller, F. Janetzko, Th. Bredow, K. Wandelt, and H. Dosch, *Phys. Rev. B* **79**, 115448 (2009).

¹¹Y. Gründer, D. Kaminski, F. Golks, K. Krug, J. Stettner, O. M. Magnussen, A. Franke, J. Stremme, and E. Pehlke., *Phys. Rev. B* **81**, 174114 (2010).

¹²H. C. N. Tolentino, M. de Santis, Y. Gauthier, and V. Langlais, *Surf. Sci.* **601**, 2962 (2007).

¹³C. Y. Nakakura, V. M. Phanse, and E. I. Altmann, *Surf. Sci.* **370**, L149 (1997).

¹⁴C. Y. Nakakura, V. M. Phanse, and E. I. Altmann, *Surf. Sci.* **401**, 173 (1998).

¹⁵D. W. Suggs and A. J. Bard, *J. Phys. Chem.* **99**, 8349 (1995).

¹⁶M. R. Vogt, F. A. Möller, C. M. Schilz, O. M. Magnussen, and R. J. Behm, *Surf. Sci.* **367**, L33 (1996).

¹⁷M. R. Vogt, A. Lachenwitzer, O. M. Magnussen, and R. J. Behm, *Surf. Sci.* **399**, 49 (1998).

¹⁸P. Broekmann, W. Lisowski, M. Anastasescu, A. Spaenig, and K. Wandelt, *J. Electroanal. Chem.* **500**, 241 (2001).

¹⁹L.-Q. Wang, A. E. Schach von Wittenau, Z. G. Ji, L. S. Wang, Z. Q. Huang, and D. A. Shirley, *Phys. Rev. B* **44**, 1292 (1991).

²⁰J. G. Gordon, O. R. Melroy, and M. F. Toney, *Electrochim. Acta* **40**, 3 (1995).

²¹M. F. Toney, J. N. Howard, J. Richter, G. L. Borges, J. G. Gordon, O. R. Melroy, D. G. Wiesler, D. Yee, and L. B. Sorensen, *Nature (London)* **368**, 444 (1994).

²²M. F. Toney, J. N. Howard, J. Richter, G. L. Borges, J. G. Gordon, O. R. Melroy, D. G. Wiesler, D. Yee, and L. B. Sorensen,

- Surf. Sci. **335**, 326 (1995).
- ²³I. Danielewicz-Ferchmin and A. R. Ferchmin, *J. Phys. Chem.* **100**, 17281 (1996).
- ²⁴I. Danielewicz-Ferchmin, A. R. Ferchmin, and A. Szaferek, *Chem. Phys. Lett.* **288**, 197 (1998).
- ²⁵I.-Y. Yeh and M. L. Berkowitz, *Chem. Phys. Lett.* **301**, 81 (1999).
- ²⁶J. Zhao, C. T. Chan, and J. G. Che, *Phys. Rev. B* **75**, 085435 (2007).
- ²⁷S. Schnur and A. Gross, *New J. Phys.* **11**, 125003 (2009).
- ²⁸P. Fenter and N. C. Sturchio, *Prog. Surf. Sci.* **77**, 171 (2004).
- ²⁹I. K. Robinson, *Phys. Rev. B* **33**, 3830 (1986).
- ³⁰F. U. Renner, Y. Gründer, and J. Zegenhagen, *Rev. Sci. Instrum.* **78**, 033903 (2007).
- ³¹O. M. Magnussen, K. Krug, A. H. Ayyad, and J. Stettner, *Electrochim. Acta* **53**, 3449 (2008).
- ³²D. Kaminski, K. Krug, F. Golks, J. Stettner, and O. M. Magnussen, *J. Phys. Chem. C* **111**, 17067 (2007).
- ³³J. M. Bloch, *J. Appl. Crystallogr.* **18**, 33 (1985).
- ³⁴Ch. Brönnimann, E. F. Eikenberry, R. Horisberger, G. Hülsen, B. Schmitt, C. Schulze-Briese, and T. Tomizaki, *Nucl. Instrum. Methods Phys. Res. A* **510**, 24 (2003).
- ³⁵D. Martocchia, M. Björck, C. M. Schlepütz, T. Brugger, S. A. Pauli, B. D. Patterson, T. Greber, and P. R. Willmott, *New J. Phys.* **12**, 043028 (2010).
- ³⁶C. M. Schlepütz, M. Björck, E. Koller, S. A. Pauli, D. Martocchia, Ø. Fischer, and P. R. Willmott, *Phys. Rev. B* **81**, 174520 (2010).
- ³⁷D. T. Pham, H. Keller, S. Breuer, S. Huemann, N. T. N. Hai, C. Zoerlein, K. Wandelt, and P. Broekmann, *Chimia* **63**, 115 (2009).
- ³⁸H. Keller, M. Saracino, N. T. N. Hai, and P. Broekmann (unpublished).
- ³⁹GoF $\frac{1}{N-P} \sum_{hkl} (I_{hkl}^{\text{exp}} - I_{hkl}^{\text{calc}})^2 / \sigma_{hkl}^2$ with I^{exp} and I^{calc} : observed and calculated intensity of each reflection (hkl), σ_{hkl} : standard deviation of I_{hkl}^{exp} , N : number of data, P : number of fitted parameters.